MEASUREMENT OF TEMPERATURE DEPENDENCE OF COMPLEX SUSCEPTIBILITY AND ITS ANISOTROPY IN FERROMAGNETIC MATERIAL

Hajer LAGHA[1,3], Hafedh BELMABROUK[1,2]
[1] Laboratory of Electronics and Microelectronics, Faculty of Sciences of Monastir, University of Monastir, Tunisia
[2]Department of Physics, College of Science Al Zulfi, Majmaah University, KSA
Herve CHAZAL[3]
[3]Electrical Engineering Laboratory (G2Elab), University of Grenoble Alpes, France
Email: hkhejer@gmail.com

Abstract: *Power electronic converters play a major role in many industrial designs. The choice of the appropriate magnetic material and the analysis of the dependence of its magnetic proprieties versus the temperature are crucial for the design of magnetic components of power converters. In this work, nanocrystalline ribbons are used to perform the toroidal core simulating a convertor. We started by elaborating a theoretical model to assess the complex permeability. This model is based on Neel theory and it takes into account wall displacement and coherent rotation. Semi-analytical expressions are derived for the dynamic permeability $\mu_{\perp}(\omega)$ in the direction perpendicular to the magnetization direction and the dynamic permeability $\mu_{RD\parallel}(\omega)$ in the direction parallel to the rolling direction. An experimental set-up has been used to measure different kinds of impedance from which the permeability is deduced versus the frequency and for several temperatures. The last step consists on the identification of some parameter using the theoretical model and experimental data. The dependence of these parameters (domain susceptibility, anisotropy energy, average domain thickness, and angle between the magnetic field and the magnetization) versus the temperature is analyzed. These parameters are expected to be valuable in the design of a converter.*
Keywords: *Neel model, coherent rotation, wall displacement, complex permeability, anisotropy energy, equivalent circuit.*

1. Introduction

Power electronic converters play a major role in the field of renewable energy such as fuel cells, wind energy and water desalination [1-3]. They are also important in many industrial, aerospace and telecommunications applications [4-7]. They provide various functions such as energy transfer and storage or disturbances filtering. Their design compels many requirements and technological constraints such as the efficiency, the size, the volume, the cost, the temperature rise and the lifetime estimation of the converter components at the different stages of energy conversion. Magnetic integration is an attractive solution to satisfy these requirements. The optimization of converter magnetic components may be pursued on different lines of investigation such as the choice of the magnetic materials, the identification of the parameters that affect the global features of the components and the analysis of the thermal problems [8-14]. In this paper, we intend to measure the complex permeability of a toroidal core of nanocrystalline FeNbCuSiB alloys. The indirect measures are performed versus the frequency and at different temperatures ranging from 20 to 180 °C. A theoretical model is used to identify the domain thickness, the angle between the magnetic field and the magnetization, the domain susceptibility and the anisotropy energy from the complex permeability measurements. These parameters are useful to the design of the converter and to investigate its magnetic and thermal behaviors.

2. Theoretical Background

Nanocrystalline ribbons are used to perform the toroidal core simulating a convertor. An electromagnetic propagation wave model will be used to evaluate the complex permeability $\tilde{\mu} = \mu_0(\mu' - j\mu'')$ (where μ_0 is the vacuum permeability, μ' and μ'' are real and imaginary parts of the relative complex permeability). To take into account the non-homogeneity of the magnetic material, the domain walls description has been used [15]. We adopt the well-known Neel's model.

The following assumptions are made:

- The external magnetic field exciting the material is sinusoidal with an angular frequency ω;
- The amplitude of external magnetic field H_0 is small;
- The ferromagnetic material behaves as a linear media. Therefore, it is possible to use the concept of permeability to describe its macroscopic behavior;
- The material is anisotropic. The magnetic field $\vec{H}$ and the magnetization field $\vec{M}$ are not collinear. The angle between these two vectors is designed by α;
- The ferromagnetic film has the structure of a two-dimensional 180° Bloch-type domain wall (Fig.

1). The distance d between two consecutive domains is supposed to be constant. The thickness of the slab is designed by δ;

- Two mechanisms contribute to the magnetization, namely the wall displacement and coherent rotations;
- The direction of the magnetization field $\vec{M}$ deviates with an angle θ under the effect of the magnetic field;
- The component of the magnetic field perpendicular to the magnetization field does not apply a force on the domain walls. In other words, it does not contribute to the wall displacement.

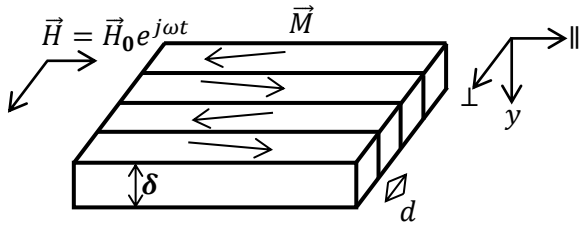

Fig. 1. Wall domains in a ferromagnetic material.

The magnetic field $\vec{H}$ may be decomposed in a basis whose directions are parallel and perpendicular to the magnetization field $\vec{M}$ (Fig. 2).

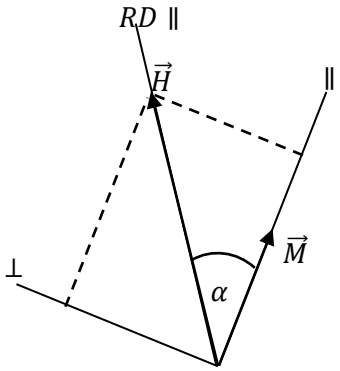

Fig. 2. Decomposition of the magnetic field into parallel and perpendicular parts due to material anisotropy.

The susceptibility is given by the matrix (χ):

$$\begin{pmatrix} \delta M_{\parallel} \\ \delta M_{\perp} \end{pmatrix} = \begin{pmatrix} \chi_{11} & \chi_{12} \\ \chi_{21} & \chi_{22} \end{pmatrix} \begin{pmatrix} \delta H_{\parallel} \\ \delta H_{\perp} \end{pmatrix} \quad (1)$$

It is also useful to decompose the vectors on the axis parallel and perpendicular to the rolling direction (RD). It is straightforward to obtain the susceptibility matrix χ_{RD} in this basis from the matrix (χ) and the angle α. It is also worthwhile to relate each term to the effect of wall displacement or coherent rotations. For instance, we have

$$\chi_{11} = \left(\frac{\delta M_{\parallel}}{\delta H_{\parallel}} \right)_{\delta H_{\perp}=0} \quad (2)$$

In other terms, this term is equal to that obtained by the wall displacement model [16]. Regarding the third term, we obtain $\chi_{21} = 0$ since the component $H_{\parallel}$ cannot provoke any magnetization variation in the perpendicular direction. The terms χ_{12} and χ_{22} are due to coherent rotations. Magnetic field diffusion equation is written for the components $H_{\parallel}$ and $H_{\perp}$. To resolve these equations, one should add the boundary conditions. The general solution may be obtained using a Fourier series decomposition. A laborious technique has been detailed by [16]. The dynamic permeability $\mu_{\perp}$ in the direction perpendicular to the magnetization direction is given by:

$$\mu_{\perp}(\omega) = \frac{\tanh(X)}{X} \mu_{\perp} \quad (3)$$

$$X = \frac{\delta}{2} \sqrt{j\omega\sigma\mu_0\mu_{\perp}} \quad (4)$$

σ is the electrical conductivity of the material and $\mu_{\perp}$ is scalar real permeability. It should be noted that $\mu_{\perp}$ depends on the anisotropy energy Ku [16]. The dynamic permeability $\mu_{RD\parallel}$ in the direction parallel to the rolling direction is given by:

$$\mu_{RD\parallel}(\omega) = 4\mu_0 \frac{\chi_w}{d} A^2 \cos^2(\alpha) + \mu_0 \mu_{\perp}(\omega) \sin^2(\alpha) \quad (5)$$

χ_w is the domain susceptibility of the material. It is related to the initial static susceptibility of the material. The parameter A depends on the coefficients of the Fourier series decomposition. Its expression is available in [16]. It is also worthwhile to write the relation for the susceptibility at low frequencies. The above relations allow to compute the permeability $\mu_{RD\parallel}(\omega)$ and the permeability $\mu_{\perp}(\omega)$ versus the frequency when the parameters χ_w, d, $\mu_{\perp}$, α, σ and δ are known. On the other hand, the measurement of the real part and imaginary part of the permeability $\mu_{RD\parallel}(\omega)$ leads to the identification of these parameters using a nonlinear algorithm. It should be noted that the temperature does not appear explicitly in the above model. However, the parameters involved may depend on the temperature. For this reason, the experiments will be done at different temperatures to analyze the dependence of the identified parameters versus the

temperature.

3. Experimental Set Up

The permeability of the material will be measured indirectly. Indeed, we will perform some impedance measurements from which we will deduce the permeability as we will show hereafter. A toroidal core of 20 µm nanocrystalline ribbons will be used to measure indirectly the permeability of the material. The numbers of turns of the primary and secondary windings are respectively noted N_p and N_s. The geometrical features of the toroidal core to be tested are summarized in Table 1. Primary and secondary windings are wound in diametrical CMC topology to carry out mutual impedance measurement [17, 18].

Table 1: Geometric parameters of the toroidal core

Inner diameter (mm)	10.7
Outer diameter (mm)	17
Average length L_m (mm)	43.5
Height (mm)	6.2
Cross section area A_E (mm^2)	15.6
Primary number of turns N_p	11
Secondary number of turns N_s	7

Several techniques are available to measure the impedance. In this work, we used the Agilent 4294A impedance analyzer. This device combines 4-terminal pair measurement method into an auto-balanced bridge circuit [19, 20]. The Agilent analyzer indicates modulus and argument of each impedance measurement.
Open-short compensation has been performed out before starting the measurements process to avoid wiring impact. The Agilent analyzer allows many kinds of impedance measurement such as open-circuit and short-circuits impedances. More details on the device are available in the technical documentation of Agilent [20]. Measurements are made at different temperatures from 20 °C to 180 °C using thermal chamber and at different frequencies from 40 Hz to 110 MHz. These measurements are made at each temperature by using an experimental test bench. The test bench consists of the following equipment as shown in Fig 3:

- PC (data acquisition module);
- Agilent 4294A with test fixture 1604E (40 Hz to 110 MHz);
- Thermal chamber (20 °C to 180 °C).

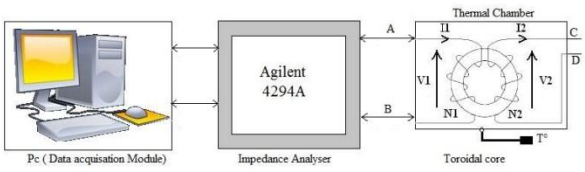

Fig. 3. Experimental set-up.

To deduce the complex permeability at given frequency and temperature many impedance measurements are performed. The experimental protocol is well explained in the provider documentation [20, 21]. As shown in Fig. 3, the toroidal core possesses 4 linked ports A, B, C and D. The analyzer allows the measurements of the 4 following impedances Z_o, Z'_o, Z_s, Z'_s: Z_o is the impedance seen from the primary when secondary winding is open circuited, Z_s is the impedance seen from the primary when secondary winding is short circuited, Z'_o is the impedance seen from the secondary when primary winding is open circuited and Z'_s is the impedance seen from the secondary when primary winding is short circuited. The confidence factor [22] is introduced to qualify measurement reliability. This factor is a useful evaluator and is defined by:

$$CF = \left| \frac{Z_o Z'_s}{Z'_o Z_s} \right| \tag{6}$$

This quantity should be equal to 1 whatever the frequency. Any deviation from the unity is a sign of measurement errors.

4. Results and Discussion

The approach adopted in this work is divided into four steps:

- First, we will present the experimental results related to the variations of the complex impedances Z_o, Z'_o, Z_s and Z'_s versus the frequency and at several temperatures ranging from 20 °C to 180 °C;
- Then, we deduce the mutual impedance Z_{12} of the quadrupole as well the magnetizing inductance Z_p and the leakage inductance Z_f of the equivalent circuit;
- After that, we deduce the complex permeability at different temperatures;
- Finally, we use the experimental data and the semi-analytical model to identify fit parameters at each temperature. Variations of these parameters versus temperature are analyzed.

4.1. Impedance measurement

Fig. 4 shows the modulus of the impedances Z_o, Z'_o, Z_s and Z'_s versus the frequency f. As mentioned above, these quantities are the impedances seen from primary and secondary winding in open circuit and short circuit operating conditions. The temperature related to this figure is T = 20 °C. To obtain this measurement, the oscillator level is fixed at 5 mV. The dotted lines in this figure represent respectively the impedance of 10 nH inductor and a 1 pF capacitor. They give a rough idea of resolution limits

of equipment used. It is clear the open impedances are grater then short circuit impedances. Fig 4 shows that impedances varies in a large range when the frequency increases. For large frequencies, the open circuit impedances reach their maximal values then decrease.

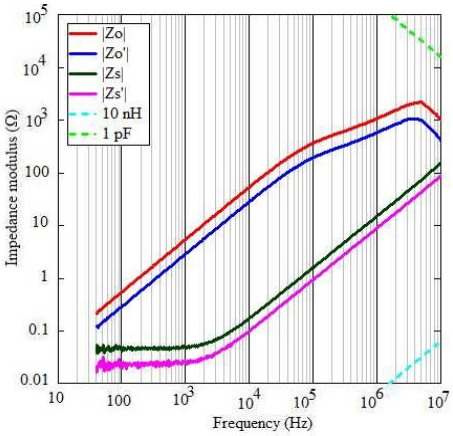

Fig. 4. Open and short circuit impedance modulus at 20 °C.

To further characterize the toroidal core, we can compute the mutual impedance Z_{12} using the following relation [23, 24]:

$$Z_{12}(\omega) = \sqrt{Z_o'(Z_o - Z_s)} \qquad (7)$$

Fig 5 shows the mutual impedance modulus at T = 40 °C and T = 180 °C. This mutual impedance is deduced from two open-circuits and one short-circuits measurements. We notice the variation in slope between 1 MHz and 10 MHz on the impedance modulus at T = 180 °C. During the data acquisition, noise appears in Fig 5 at low and high frequencies. The mutual impedance shows a change in its trend. It reaches a maximum value then it starts to decrease.

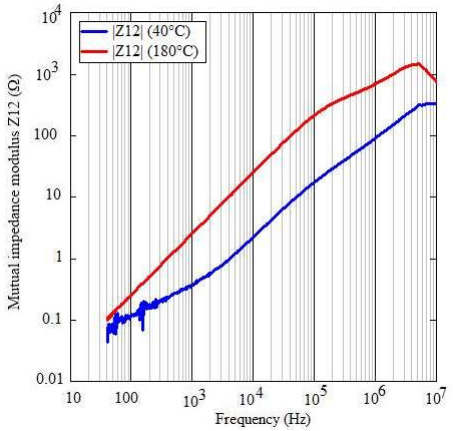

Fig. 5. Mutual impedance versus frequency for two values of temperature.

The toroidal core is modeled by a lumped element circuit by using impedance measurements (Fig 6). This equivalent circuit includes two serial resistances r_1 and r_2 as well as a magnetizing inductance Z_p and leakage inductance Z_f. The dc resistances r_1 and r_2 are obtained respectively from Z_o and Z_o' curves at low frequencies. The other measured quantities Z_s and Z_s' are used to evaluate magnetizing inductance Z_p and leakage inductance Z_f. The magnetizing inductance is given by:

$$Z_p(\omega) = \frac{Im(Z_o - r_1)}{2\pi f} \qquad (8)$$

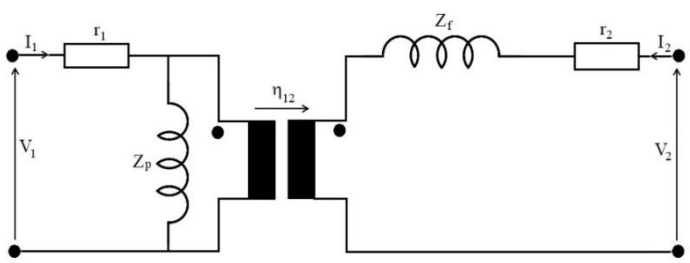

Fig. 6. Two windings transformer.

Fig 7 shows the magnetizing inductance versus frequency and for two values of temperature. The magnetizing inductance decreases when the frequency increases. The effect of temperature is pronounced at low frequencies. However, at large frequencies, the two curves become identical i.e. the effect of temperature vanishes. The magnetizing inductance reached a peak around 5.6×10^{-4} H at T = 180 °C and 8.69×10^{-4} H at T = 40 °C.

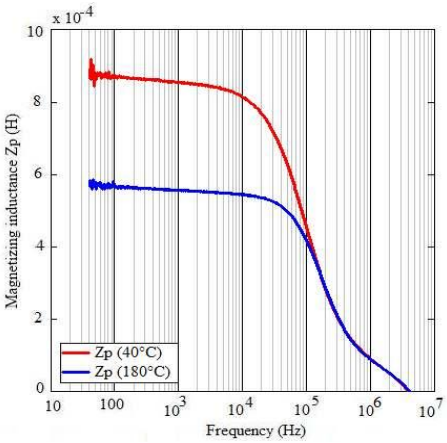

Fig. 7. Magnetizing inductance versus frequency at T = 40 °C and T = 180 °C.

4.2. Complex permeability

The above measurements allow us to deduce the

complex permeability of the toroidal core made from the nanocrystalline FeNbCuSiB alloys. According to [18] the dynamic permeability is given by:

$$\mu(\omega) \cong \frac{Z_p(\omega) L_m}{\omega N_p N_s A_E \mu_0} \qquad (9)$$

The geometrical parameters involved in Equation (9) are presented in Table 1. This equation enables us to plot the complex permeability versus the frequency at different values of the operating temperature.

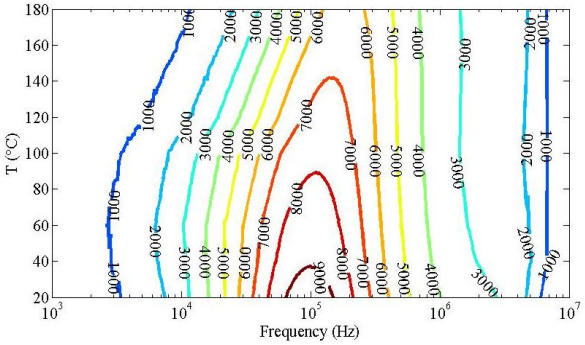

Fig. 8. Isovalue of the real part of the complex permeability μ' versus temperature and frequency.

Fig 8 shows the isovalue of the real part μ′ of the complex permeability. The maximum value of μ′ is obtained at a frequency 100 kHz and at ambient temperature. When the temperature increases, the position of the maximum value of μ′ is shifted toward high frequencies and the value of this maximum decays. In other words, the temperature increase leads to the alteration of magnetic proprieties of the alloys. For this reason, it is important to introduce the dependence of μ′ versus the frequency as well as the temperature in the design of magnetic converter. It is expected that the heat transfer inherent to the converter operation has significant effect on its performance. Therefore, it is important to take into account the magnetic and thermal proprieties of the material. Compact models should involve magnetic part as well as a thermal part [25]. In this study, the magnetic and thermal effects have been treated independently since the temperature has been considered as a parameter that can influences magnetic proprieties. Actually, the two mechanisms are coupled and we have to resolve heat transfer equation to obtain the operating temperature. The source term in this equation is relative to magnetic proprieties [25, 26].

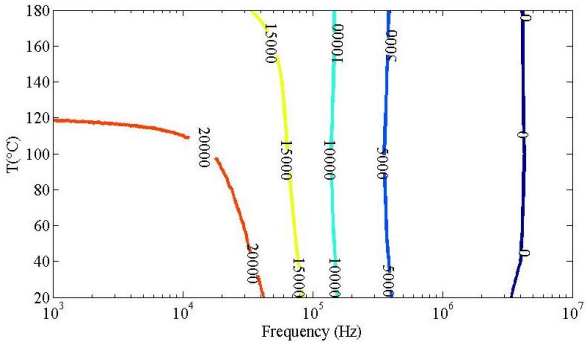

Fig. 9. Isovalue of the imaginary part of the complex permeability μ′′ versus temperature and frequency.

Fig 9 presents the isovalue of the imaginary part μ'' of the complex permeability. At large frequencies, isovalue curves are almost vertical lines. This means that μ'' does not depend on temperature. Since μ'' is mainly due to the electrical conductivity σ, we deduce that temperature does not influence the electrical conductivity at large frequencies. On the other hand, at low frequencies, the increase of temperature induces a decrease of μ'' and an increase of σ. At a given temperature, μ'' decreases monotonously versus the frequency. We deduce that heat transfer affects electrical conductivity only at low frequencies. The above abacus may be implemented as they are. It is also possible to tray to fit the experimental data by empirical correlations which are easier to use by engineers.

4.3. Identification of parameters and effect of temperature

As mentioned in section 2, the theoretical model involves some parameters which depend on frequency and temperature. These physical quantities are: the average domain thickness d, the domain susceptibility χ_w, the anisotropy energy Ku and the angle between the magnetic field and the magnetization α. The fit of experimental data using the theoretical model allows the identification of these quantities and the validation of the model. To simplify the identification procedure we will start by analyzing the behavior of the permeability at low frequencies. This step allows us to identify the anisotropy energy Ku and the angle between the magnetic field and the magnetization α. In the second step, we use all the permeability curve to identify unambiguously the average domain thickness d and the domain susceptibility χ_w. An iterative algorithm has been elaborated and validated to perform this task. A bloc diagram of the algorithm is given in Fig. 10. The algorithm is also based on minimization of errors using least squares method.

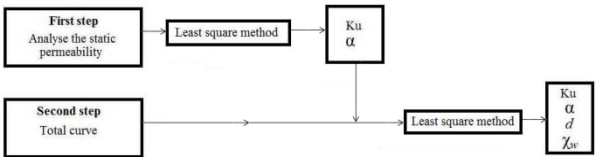

Fig. 10. Bloc diagram of optimization model

Fig 11 shows the comparison of the real part μ′ and the imaginary part μ′′ of the complex permeability at three values of temperature. It is clear that the theoretical model fits well the experimental data. This result validates the identification process.

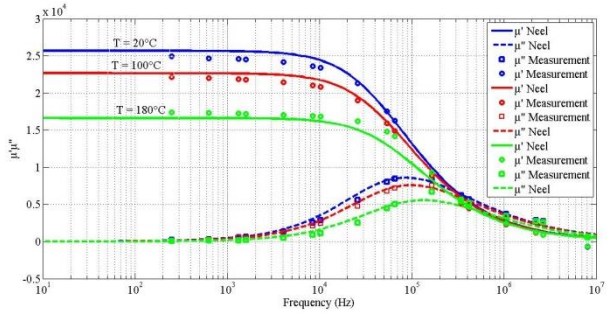

Fig. 11. Complex permeability spectra deduced at different temperatures.

Fig 12 exhibits the variation of anisotropy energy versus the temperature. It is clear that the anisotropy depends strongly on temperature. It declines from 1200 J/m^3 at 20 °C to 400 J/m^3 at 180 °C. As the temperature approaches the Curie point, the material becomes more and more isotropic. A similar behavior has been observed for some materials such as magnetite (Fe_3O_4) (Curie point 280 K) [27] and nanoparticles ($MnFe_2O_4$) (Curie point 125 K) [28]. The obtained result proves that thermal heating of a converter has an important effect on the anisotropy energy. This finding suggests that heat transfer is expected to impact strongly magnetic performance of a converter and it is necessary to develop new models that are able to deal simultaneously with magnetic and thermal mechanisms.

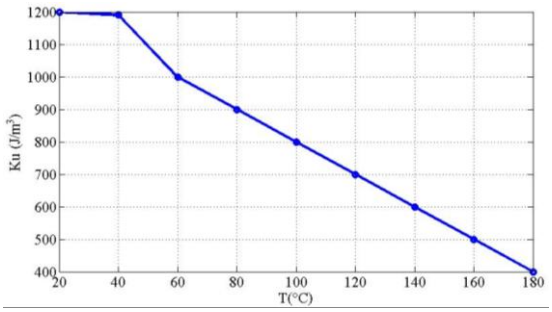

Fig. 12. Anisotropy energy versus temperature.

Fig 13 shows the temperature dependence of the magnetic susceptibility for the FeNbCuSiB alloys. The domain susceptibility decreases with increasing temperature from 1.7×10^5 at 20 °C to 10^5 at 180 °C. This variation should be interpreted as a consequence of the anisotropy energy difference between the transforming phases and indicated the presence of a transition form.

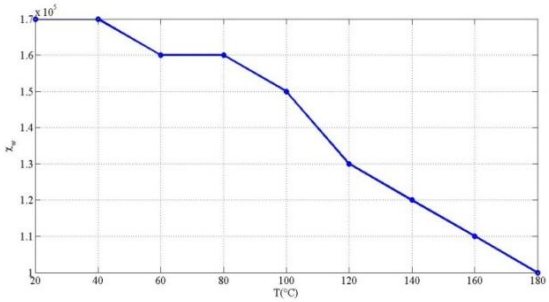

Fig. 13. Domain susceptibility versus temperature.

Fig 14 and Fig 15 show the temperature independence of the average domain thickness d and the angle between the magnetic field and the magnetization α. Indeed, the quantities d and α remain constant at different temperatures. This behavior may be explained by the absence of mechanical stress on our material. The quantities d and α are then intrinsic material proprieties.

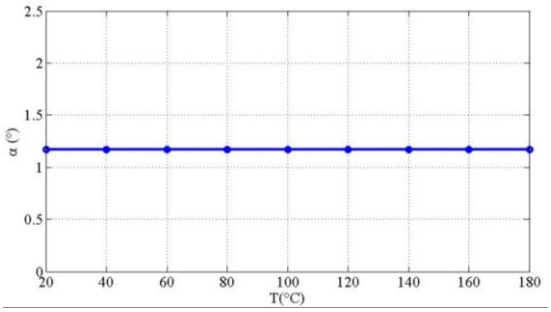

Fig. 14. Angle α versus temperature.

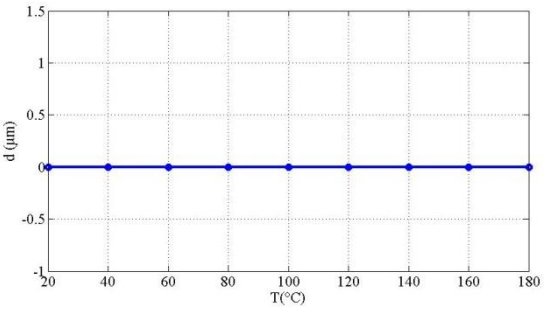

Fig. 15. Average domain thickness versus temperature.

5. Conclusion

In this paper, a theoretical model is proposed to

describe the magnetic structure of ferromagnetic materials. The medium is assumed to be linear but anisotropic. The contribution of wall displacement and coherent rotation are considered. The semi-analytical model allows to determine the complex permeability versus the frequency. In order to check the reliability of the theoretical model and in particular the evolution of the physical parameters with respect to the temperature, experimental measurements have been done on a nanocrystalline material. They consist to characterize its magnetic behavior using four experimental impedance measurements. The variations of some parameters are studied as a function of temperature. These parameters are the average domain thickness, the angle between the magnetic field and the magnetization, the domain susceptibility and the anisotropy energy. The experimental results reveal the effect of temperature on these parameters. The model elaborated and the experimental results obtained are expected to provide valuable information for engineers. They can be implemented in a compact model to simultaneously simulate the magnetic behavior of power electronic converter and take into account thermal effects.

References

1. Ahmed, O.A., Bleijs, J.A.M.: *An overview of DC–DC converter topologies for fuel cell-ultra capacitor hybrid distribution system*. In: Renewable and Sustainable Energy Reviews, vol.42 (2015), p. 609-626.
2. Kolli, A., Gaillard, A., De Bernardinis, A., Bethoux, O., Hissel, D., Khatir, Z.: *A review on DC/DC converter architectures for power fuel cell applications*. In: Energy Conversion and Management, vol.105 (2015), p. 716-730.
3. Holtsmark, N., Agheb, E., Molinas, M., Høidalen, H. K.: *High frequency wind energy conversion system for offshore DC collection grid — Part II: Efficiency improvements*. In: Sustainable Energy, Grids and Networks, Article in press
4. Naayagi, R. T., Forsyth, A. J., Shuttleworth, R.: *Performance analysis of extended phase-shift control of DAB DC-DC converter for aerospace energy storage system*. In IEEE Power Electronics and Drive Systems, 2015, p. 514-517.
5. Soliman, H., Wang, H., Blaabjerg, F.: *A Review of the condition monitoring of capacitors in power electronic converters*. In: IEEE International ACEMP-OPTIM-ELECTROMOTION JOINT Conference, (2015), p. 243-249.
6. Naayagi, R. T.: *Selection of power semiconductor devices for the DAB DC-DC converter for aerospace applications.* In: IEEE Power Electronics and Drive Systems, 2015, p. 499-502.
7. Wrzecionko, B., Kolar, J. W., Looser, A., Casey, M.: *High-temperature (250 °C / 500 °F) 19 000 min-1 BLDC fan for forced air-cooling of advanced automotive power electronics*. In: IEEE ASME Transactions on Mechatronics, vol.20 (2015), p. 37-49.
8. Ghodake, J.S., Shinde, T.J., Patil, R.P., Patil, S.B., Suryavanshi, S.S.: *Initial permeability of Zn–Ni–Co ferrite.* In: Journal of Magnetism and Magnetic Materials, vol.378, (2015), p. 436-439.
9. Wang, Y. K., Zhou, Y., Zhai, Y., Xiao, J. Q.: *High-frequency magnetic properties Fe–Hf–B–O ribbons with chromium additive*. In: IEEE Transactions On Magnetics, vol.51 (2015), No.11, p. 1-3.
10. Cuellar, C., Idir, N., Benabou, A.: *High-frequency behavioral ring core inductor model.* In: IEEE Transactions on Power Electronics, vol.31 (2016), No. 5, p. 3763-3772.
11. Prasanth, V., Bauer, P., Ferreira, J.A., Polinder, H.: *Review of analytical methods to extract magnetic parameters of an inductively coupled circuit*. In: IEEE Emerging Technologies: Wireless Power (WoW), (2015), p. 1-8.
12. Hilal, A., Raulet, M. A., Martin, C., Sixdenier, F.: *A Comparative study: dynamic and thermal behavior of Nanocrystalline and Powder magnetic materials in a power converter application.* In: Journal of Electronic Materials, vol. 44 (2015), No. 10, p. 3768-3776.
13. You, B.G., Ko, J.M., Kim, J.H., Lee, B.K.: *Proposal of potted inductor with enhanced thermal transfer for high power boost converter in HEVs*. In: Journal Electrical Engineering & Technology), vol.10 (2015), p.30-40.
14. Hilal, A., Raulet, M. A., Martin, C., Sixdenier, F.: *Power loss prediction and precise modeling of magnetic powder components in DC-DC power converter application*. In: IEEE Transactions on Power Electronics, vol.30 (2015), No. 4, p. 2232-2237.
15. Ahmadi, B., Chazal, H., Waeckerle, T., Roudet, J.: *Studying behavior of multilayer materials: A 1-D model correlated to magnetic domain walls through complex permeability*. In: Journal of Magnetism and Magnetic Materials., vol.320 (2008), p. e708-e711.
16. Ahmadi, B., *Composant magnétique intégré en alliage FeNiCrCu pour l'électronique de puissance*, Ph.D. thesis, University of Grenoble, 2010.
17. Mesmin, F., Ahmadi, B., Chazal, H., Kedous Lebouc, A., Sixdenier, F.: *Improving reliability of magnetic mutual impedance measurement at high excitation level*. In: IEEE International Instrumentation and Measurement Technology Conference, China, 2011, p. 1.
18. Mesmin, F.: *Matériaux magnétiques et solutions innovantes de filtrage CEM pour applications aéronautiques*, Ph.D. thesis, University of Grenoble, 2012.
19. Agilent Impedance Measurement Handbook, A guide to technology and techniques, 4th Edition. (Agilent Technologies, USA, 2009)
20. Agilent 16454A Magnetic Material Test Fixture, Operation and service manual, Fifth Edition. (Agilent Technologies, USA, 2001)
21. Margueron, X.: *Elaboration sans prototypage du circuit équivalent de transformateurs de type planar*, Ph.D. thesis, University of Grenoble, 2006.
22. Besri, A., Chazal, H., Keradec, J. P., Margueron, X.: *Using confidence factor to improve reliability of wide frequency range impedance measurement. Application to H.F. transformer characterization*. In: IEEE

Instrumentation & Measurement Technology Conference, Singapore, Singapore, 2009, p.104-109.
23. Sakhno, L., Sakhno, O., Dubitsky, S.: *Field-circuit modelling of an advanced welding transformer with two parallel rectifiers*. In: Archives of Electrical Engineering, vol.64 (2015), No. 2, p. 249-257.
24. Taher, A., Sudhoff,S., Pekarek S.: *Calculation of a tape-wound transformer leakage inductance using the MEC model*. In: IEEE Transactions on Energy Conversion, vol.30 (2015), No. 2, p. 541-549.
25. Lagha, H., Chazal, H., Belmabrouk, H.: *A new approach for generating compact thermal models*, in: International Conference on Electrical Sciences and Technologies, Tunisia, 2014, p. 1-7.
26. Nasri, F., Echouchene, F., Ben Aissa, M. F., Graur, I., Belmabrouk, H.: *Investigation of self-heating effects in a 10-nm SOI-MOSFET with an insulator region using electrothermal modeling*. In: IEEE Transactions Electron Devices, vol.62 (2015), No. 8, p. 2410-2415.
27. Yoon S.: *Determination of the temperature dependence of the magnetic anisotropy constant in magnetite nanoparticles*. In: Journal of the Korean Physical Society, vol.59 (2011), No. 5,p. 3069-3073.
28. Yoon S., Krishnan K.M.: *Temperature dependence of magnetic anisotropy constant in manganese ferrite nanoparticles at low temperature*. In: Journal of Applied Physics, vol.109 (2011), No. 07B534, p. 1-3.